EVALUATION OF BUNDLE BLOCK ADJUSTMENT FOR 3D GEOSPATIAL MODELLING USING UAV-BASED SMALL-FORMAT MULTI-HEAD CAMERA SYSTEMS

Thirawat BANNAKULPIPHAT – Ph.D Student, Technische Universität Wien, Faculty of Mathematics and Geoinformation, Department of Geodesy and Geoinformation, Austria – Researcher, Chulalongkorn University, Mapping and Positioning from Space (MAPS) Technology Research Center, Department of Survey Engineering, Thailand, thirawat.bannakulpiphat@geo.tuwien.ac.at
Wilfried KAREL – Senior Scientist, Dipl.-Ing.,Technische Universität Wien, Faculty of Mathematics and Geoinformation, Department of Geodesy and Geoinformation, Austria, wilfried.karel@geo.tuwien.ac.at
Camillo RESSL – Senior Scientist, Dipl.-Ing. Dr.techn.,Technische Universität Wien, Faculty of Mathematics and Geoinformation, Department of Geodesy and Geoinformation, Austria, camillo.ressl@geo.tuwien.ac.at
Norbert PFEIFER – Univ. Prof., Dipl.-Ing. Dr.techn., Technische Universität Wien, Faculty of Mathematics and Geoinformation, Department of Geodesy and Geoinformation, Austria, norbert.pfeifer@geo.tuwien.ac.at

***Abstract**: Aerial oblique imaging is increasingly used for high-resolution 3D geospatial data collection, particularly in urban environments. Multi-head camera systems, which integrate both nadir and oblique cameras, offer enhanced geometric coverage. The small-format multi-head camera system used in this study is designed to be lightweight and compact. However, this compactness introduces inherent limitations, resulting in trade-offs such as reduced ground coverage, limited geometric overlap betweenviewing directions, and constraints on integrating high-precision instruments like GNSS and INS. In this paper, we focus on relative orientation by evaluating image connectivity, image ray intersection, tie point multiplicity and accuracy. Our objective is to improve accuracy and optimize photogrammetric workflows by enhancing precision, reliability, automation, and efficiency, ultimately leading to higher-quality 3D reconstructions and mapping results also from small-format multi-head camera systems.*

***Keywords:** Small-Format; Oblique Camera; Multi-Head Camera Systems; Bundle Block Adjustment*

1. Introduction

Aerial oblique imaging has become increasingly popular for high-resolution 3D geospatial data collection, particularly in urban environments. This technique supports applications such as building information modelling (BIM), urban planning, and infrastructure development. Multi-head camera systems, which integrate both nadir and oblique cameras, are of particular interest, as they provide more comprehensive geometric coverage. This significantly enhances the interpretation and classification of terrain features by capturing images from multiple angles, thereby improving 3D modelling accuracy and increasingmapping accuracy [1,2,3].

In UAV-based photogrammetry for aerial mapping, the weight and size constraints of cameras are critical factors, as minimizing them is essential not only for efficient and effective surveying and mapping tasksbut also for complying with legal restrictions - lighter systems often face fewer regulatory constraints regarding flight permissions.Small-format cameras, which are lightweight and compact, are suitable for UAV mounting. However, they involve trade-offs due to the inherent limitations of their compact size. These cameras typically rely on low-quality GNSS (Global Navigation Satellite Systems) data and lightweight, or even non-existent, INS (Inertial Navigation Systems), resulting in reduced accuracy in direct geo-referencing of single images. This contrasts with larger, metric, and more robust camera systems that can be equipped with high-quality INS and GNSS, thereby enhancing positioning accuracy. The “small-format” camera system used in this study is especiallycompact and lightweight. The entire system measures approximately 145 mm × 145 mm × 105 mm and weighs 840 g, making it well-suited for UAV-based aerial surveying. Therefore, evaluating various computational factors of small-format multi-head camera systems in UAV-based mapping and surveying applications, particularly those that influence performance and the quality of derived products, is essential.Although a few publications have investigated the use of this camera type in the context of bundle block adjustment [4,5,6], this study builds upon and extends those works.

This paper focuses on relative orientation, a key factor in ensuring the consistency of derived information. We evaluate image connectivity, image ray intersection angle, tie point multiplicity and accuracy in penta-camera (nadir and oblique) setups, incorporating control points to enhance accuracy and ensure georeferencing. Our aim is to understand accuracy in order to optimize workflows by improving precision, reliability, automation, and speed, ultimately leading to improved 3D reconstructions and mapping outcomes using small-format multi-head camera systems.

2. Material and Method

2.1 Survey and Study Area

The study area is located in Saraburi Province, Thailand. The aerial images were acquired using the JOUAV CA502R small-format multi-head camera system. This system consists of one nadir camera and four 45-degree oblique cameras, collectively referred to as a penta-camera in this paper. Each of the five cameras has a resolution of 24 MP (6000 × 4000), resulting in a total combined resolution of 120 MP.

The camera system was mounted on a VTOL UAV, as shown in Fig.1a, and operated at a flight altitude of 150 m above ground level over a 1.0 km² area. The survey captured a total of 6,065 images, averaging 1,213 images per camera, with an 80% forward and side overlap, referring specifically to the nadir images. Data collection was conducted across two flight missions. To ensure continuity between missions and avoid any gaps, overlapping strips were captured, resulting in double image coverage in the overlap zones. The ground sampling distance (GSD) for the nadir view was 3 cm. The survey was supported by 48 ground control points (GCPs), measured using RTK-GNSS, achieving a mean positional accuracy of 5 cm. The study area, including the distribution of GCPs, is illustrated in Fig.1b.

2.2 Data Processing

The data were processed using OrientAL software [7], developed by the Department of Geodesy and Geoinformation at TU Wien, Austria. OrientAL provides a robust Structure

from Motion (SfM) pipeline that includes feature point extraction, description, and matching. It also incorporates gross error detection through essential matrix filtering with RANSAC [8] and a M-estimator for bundle block computation. The software refines image orientation through an incremental bundle block adjustment.

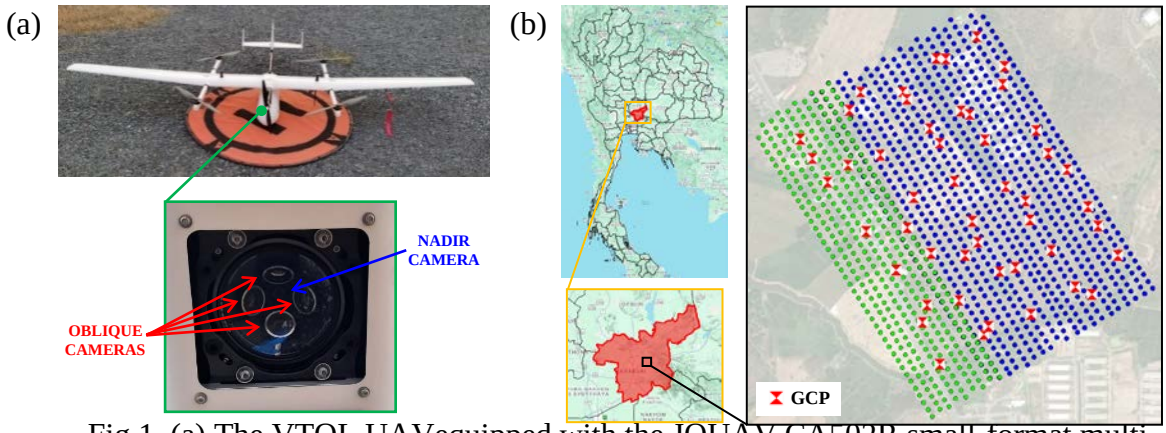

Fig.1. (a) The VTOL UAVequipped with the JOUAV CA502R small-format multi-head camera system. (b) Distribution of control points within the study area,along with camera positions fromflight mission 1 (blue circles) and flight mission 2 (green circles).

Moreover, OrientAL supports the integration of observed control points into the bundle adjustment process and the modelling of multi-head camera systems, enhancing flexibility and accuracy in photogrammetric image orientation, camera calibration, and object reconstruction. These capabilities ensure precise and reliable image processing. Fig.2 illustrates the image orientation alongside the reconstructed sparse point cloud in model space.

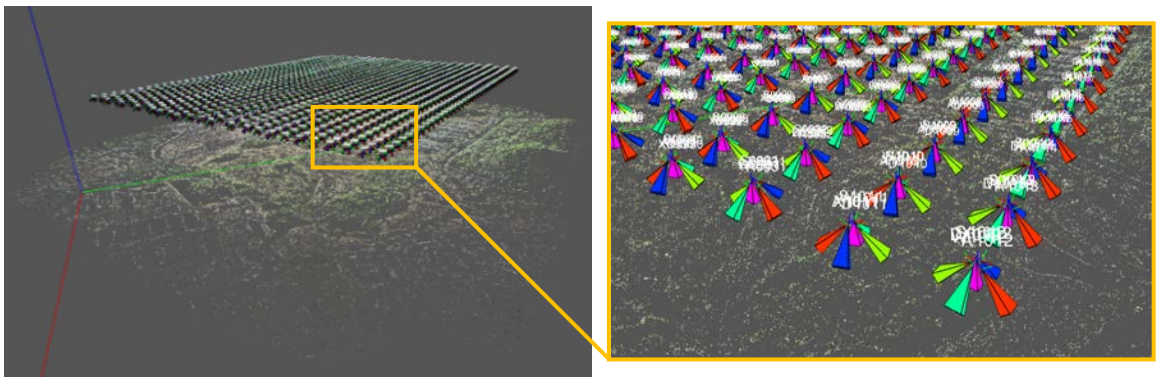

Fig. 2. Image orientations and the reconstructed sparse point cloud from the penta-camera system.

2.3 Feature Point Selection and Network Optimization Processing

As part of the photogrammetric workflow, this paper defines image connectivity as the number of corresponding points between image pairs. An ideal distribution of image connectivity should be proportional to the overlapping area (in image space), following the “von Gruber” concept. Given the limitations of IT resources, the number of tie points must be restricted in large bundle blocks[9].Nevertheless, it remains essential to achieve precise and unbiased orientation estimates efficiently and within a short time.

To address this, the feature point selection process in this study is designed to achieve two key objectives: (1) to favor tie points with higher multiplicity, which contribute to increased network robustness and overdetermination without increasing the number of unknowns, and (2) to ensure a well-connected image network with a homogeneous spatial distribution of tie points across the entire block. These goals are critical for the precise and reliable estimation of orientation parameters.

This research adopts the approach proposed in Karel et al. [9] for feature point reduction while ensuring a homogeneous distribution across the image space and favoring high-multiplicity tracks. A grid is overlaid on each image, and a target number of points is defined per cell. The selection process begins with an empty list of tracks to be kept and a counter initialized to zero for each grid cell. All tracks are sorted in descending order by their multiplicity. For each track, the grid cells of its image points are identified, and their current counts are checked. If any cell count is below the target, the track is added to the retained list and the counters for the affected cells are updated accordingly. This method ensures spatial balance while prioritizing tracks that provide greater geometric robustness.

This approach reduces point density in oversampled areas while preserving sparsely covered regions and maintaining the geometric stability of the photogrammetric network. While it reduces redundancy, the primary goal is to minimize the number of unknowns while retaining sufficient redundancy. This improves processing efficiency and supports the generation of precise, stable orientation estimates across large image blocks.

2.4 Simulation-Based Residual Analysis

To evaluate the behavior of image residuals under idealized conditions, a simulation-based bundle block adjustment was conducted. The goal of this simulation is to isolate the impact of random measurement errors and assess their influence on residual statistics, particularly in relation to tie point multiplicity.

For this purpose, image measurements were made error-free by adding the residuals back to the original measurements. A bundle block adjustment using these “corrected measurements” results in all residuals being estimated as zero. Random measurement errors were then added to these corrected measurements, drawn from a normal distribution with a mean of zero and a standard deviation equal to the sigma naught of the original adjustment. This processgenerated new residuals influenced solely by random error.

The residual length per tie point multiplicity, derived from the simulated bundle block adjustment, closely followed the shape of the following expression: $\frac{1}{m}(\sigma \cdot \sqrt{\frac{\pi}{2}}(m-2,$ where is the number of contributing images and is the image coordinate measurement precision.

The first term, ($\sigma \cdot \sqrt{}$), represents the expected value of a Rayleigh distribution, where the factorof accounts for the contributions of the third and subsequent images. Each additional image contributes a residual vector of length .The Rayleigh distribution describes the magnitude of a vector formed by combining two independent, normally distributed variables with zero mean and equal standard deviation.

The second term, ( ), corresponds to the expected value of the absolute value of a normally distributed variable with zero mean and standard deviation of sigma. This represents the residual value expected from a forward intersection using two images. In this case, the overdetermination is only 1, meaning four residuals share one normally distributed residual.

Finally, the multiplication by accounts for the averaging of all these residual vector lengths, providing a predicted baseline for residual behavior across varying tie point multiplicities.

3. Results and Discussions

3.1 Image Connectivity

In this study, we analyze image connectivity using the compass direction frame [6], with respect to continuous and stable ground coverage. As sensors, particularly multi-head cameras, collect data, the platform's view changes according to the flight direction. Notably, with each captured strip, the two pairs of opposite oblique cameras switch their viewing directions, while the compass direction remains constant. This alignment with the flight path, similar to the nadir camera, facilitates easier interpretation and analysis.

Due to the large number of images within the block, we first divided the entire block into a5 × 5 grid (Fig. 3a) before analyzing image connectivity. This method, referred to as super image connectivity, aggregates multiple images within each grid cell to form a single representative "image", along with the corresponding tie points. Fig. 3b illustrates the super image connectivity matrix of the block. Eachelement refers to a super image with a specific viewing direction. The matrix is orders by viewing directions, and within each 25×25 sub-block, thin grey lines distinguish individual strips of super images.This approach provides an overview of connectivity strength and density across a large dataset.

The colors in the super image connectivity matrix represent the number of corresponding points between grid pairs on a logarithmic scale, with the percentage of corresponding points and number of empty cells displayed at the center of each block. An empty cell indicates that no matching points were found. The diagonal of the super image connectivity matrix represents image pairs with the same viewing direction.

Most same-view pairs exhibit consistent and strong connectivity patterns.However, the SE–SE and NW–NW pairs show noticeably higher connectivity.In contrast the side views (NE-NE and SW-SW pairs) show connections only with their immediate neighboring super-strips - defined here as groups of flight strips that fall within the same vertical column of the grid - but not beyond. This is attributed to the rectangularlayout of the grid cells - specifically, a larger number of images along the flight direction (strips) compared to the cross-strip viewing direction. This configuration results in increased overlap, a greater number of tie points, and consequently, stronger connectivity for the side-viewing super images.Additionally, the camera's frame geometry, particularly the footprint overlap, contributes to enhanced forward- and backward-looking coverage in the SE and NW directions. This overlap slightly exceeds that of the nadir view, capturing a wider area and further increasing the number of corresponding points in these directions.

The diagonal of the matrix consistently shows higher connectivity than off-diagonal elements, with the Na–Na pair exhibiting the strongest match rate at 9.65%. Other same-direction pairs also display strong connectivity, such as SE–SE at 9.12% and SW–SW at 8.62%, highlighting the robustness of tie point matching when the viewing angles are consistent.In contrast, pairings between different viewing directions, as represented by the off-diagonal elements, demonstrate lower connectivity. For instance, SW–NW, which represent 90-degree differences in viewing direction, show at 5.58%. Even lower values are observed in 180-degree pairings, such as NE–SW at 3.70%. Pairings between nadir and compass direction views fall somewhere in between, with NW–Na at 6.83% and NE–Na at 6.03%. Several blocks, particularly those with opposing compass directions, also contain empty or near-empty cells due to the lack of common fields of view, making feature matching

geometrically impossible. Overall, the ranking of connectivity strength from highest to lowest is: same-direction pairs, nadir–compass direction pairs, 90-degree difference pairs, and 180-degree difference pairs.

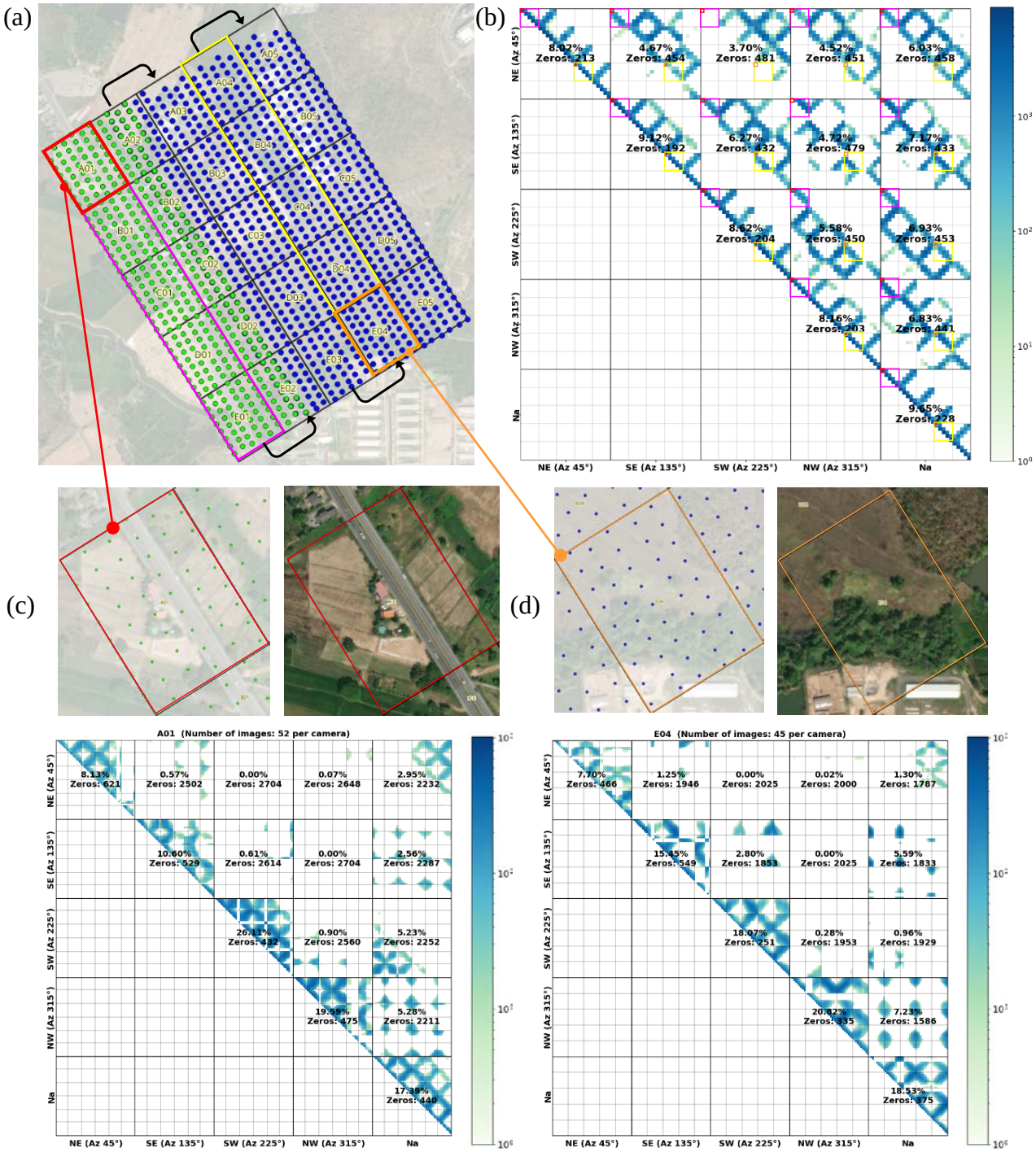

Fig. 3. (a) 5 × 5 grid division of the entire block; (b) Super image connectivity matrix of the entire block(symmetric); (c, d) Examples of image connectivity matrices in the compass direction frame (logarithmic scale). The center of each block matrix indicates the percentage of corresponding points and the number of empty cells within and across viewing directions.

A small red and orange rectangle represents an example of a single grid cell, corresponding to one pixel in the super image connectivity matrix (Fig. 3b), and indicates the image connectivity of that specific grid cell (Figs. 3c and 3d, respectively). A pink and yellow rectangle represents five grid cells located in the first and fourth columns (super-strips) of the divided block, illustrating the matrix values in terms of possible viewing direction pairs.

Considering the image connectivity of image pairs, the red and orange rectangles overlaid on selected grid cells reveal the image connectivity of all image pairs within those specific grids, consisting of 52 and 45 images, respectively.The matrix adopts a format similar to the super image connectivity matrix but differs in that each individual image contributes to one row and one column. Images with the same viewing direction are grouped into distinct blocks of rows and columns. Light grey lines separate strip-by-strip grids within each block to distinguish individual flight strips.

Figures 3c and 3d show that image pairs with the same viewing direction exhibit the highest connectivity, confirming that the overlap and side-lap percentages of the nadir camera align with the planned configuration. In contrast, 90-degree view combinations (e.g. NE–SE, SE–SW) show reduced connectivity, while 180-degree pairs frequently display zero matching points due to limited image overlap. Nadir–compass direction combinations fall in between, with values ranging from approximately 1% to 8%. These results show that different viewing directions tend to occur when the projection centers are further apart.

Overall, these variations in image connectivity arise from factors such as flight geometry, overlap and side-lap percentages, and land-use texture. However, the observed deviations suggest that connectivity does not scale linearly with image overlap, and is more strongly influenced by directional geometry and structural content within the scene.This also highlights the need for more effective strategies to establish correspondences between images captured from significantly different viewing directions. It is worth noting that the feature point selection and thinning approach proved successful in achieving a more homogeneous distribution of tie points across images.We confirmed this quantitatively through an investigation of single-camera (nadir) processing.

3.2 Image Ray Intersection Angle

The image ray intersection angle refers to the angle formed by the lines of sight from twocamera positions to a 3D point, which directly influences the precision of spatial measurements. For the cameras investigated, we derived the theoretical intersection angles and compared them to the actual intersection angles achieved. The theoretical intersection angles for all possible directional pairings between two exposure positions - nadir to nadir, oblique to oblique, and nadir to oblique - are 46°, 110°, and 78°, respectively.These values are based on idealized assumptions, including a constant flying height above ground, fixed oblique angles of 45°, and strictly nadir-looking geometry for the nadir camera.

All rays to a single tie point are used in pairs to compute the angle between the rays. For each tie point, the mean and maximum of these angles are calculated for further analysis. Fig. 4. presents the mean and maximum intersection angles for each tie point, with statistical values (mean, 25^{th}, 50^{th}, and 75^{th} percentiles).

The mean intersection angles in Fig. 4a, represented in grey, show that most tie points observed in two images have an intersection angle of approximately 12°. As the number of contributing images increases, the mean intersection angle also increases. To provide a clearer visualization, thehighest numbers of image rays per tie point were aggregatedinto compact labels. The yellow rectangle highlights a zoomed-in region, illustrating that the transition from individual values to aggregated ones remains smooth. At around 21 contributing images, the mean (blue line) and the 50^{th} percentile(median; red line), of the mean intersection angle

intersect. This indicates that below 21 images, more than half of the tie points have a mean intersection angle lower than the overall average.

In Fig. 4b, the maximum intersection anglesare color-coded based on viewing direction combinations: same viewing direction (yellow), 90-degree difference in viewing direction (blue), 180-degree difference in viewing direction (green), and compass direction paired with nadir (red) - in contrast to the grey representation in Fig. 4a. Nearlyall tie points fall below the theoretical maximum angle between oblique-to-oblique views, except for a few green points observed when the number of contributing images exceeds 12. By analyzing the color distribution associated with different intersection angles, we observe that various image pairings contribute differently as the angle increases. The color scheme reflects this: tie points from the same viewing direction generally exhibit small maximum intersection angles (yellow), while those involving compass directions and nadir views exhibit higher angles (red). Points with a 90-degree difference appear in blue, and those with a 180-degree difference correspond to the highest angle range (green).

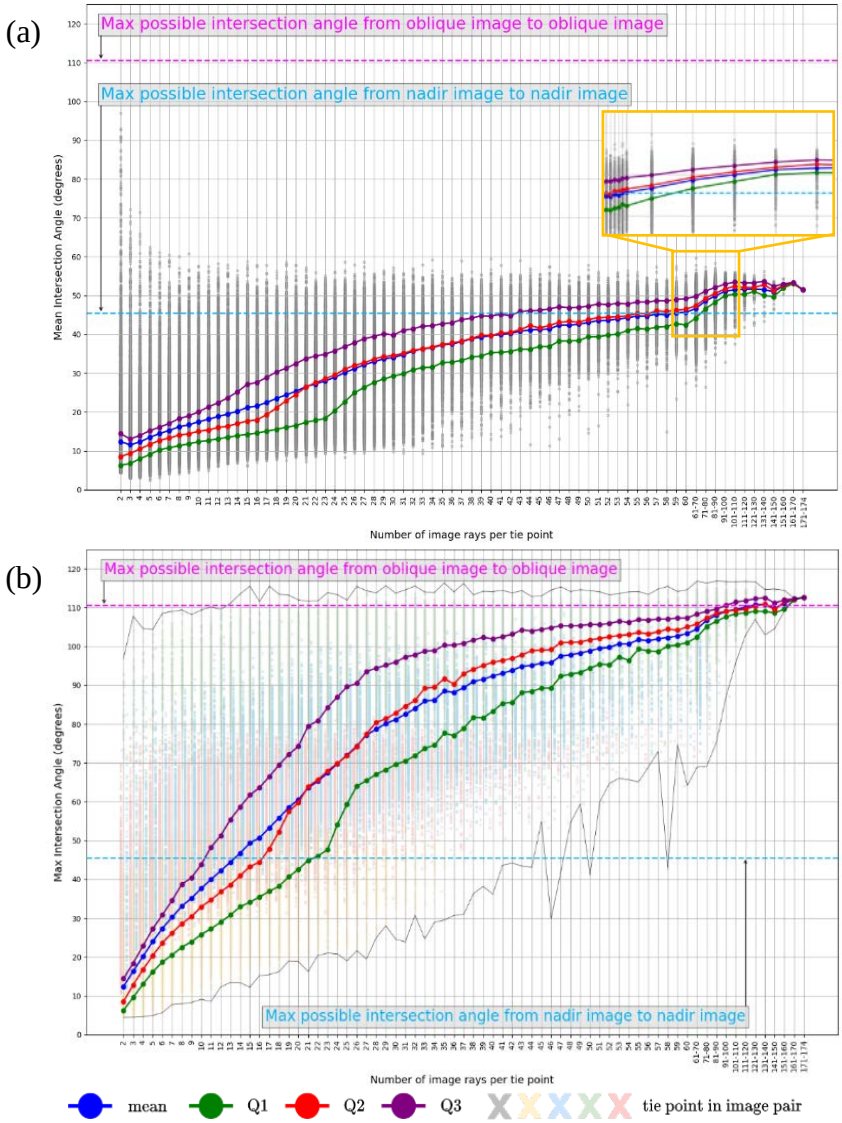

Fig.4. (a) Mean and (b) maximum image ray intersection angles for each tie point inthe penta-camera processing.Mean angles are shown in grey, while maximum angles are color-coded according to viewing direction combinations: same (yellow), 90° difference (blue), 180° difference (green), and compass–nadir (red).

Overall, the results align well with the theoretical intersection angles. Additionally, the two thin black lines in Fig. 4b represent the overall minimum and maximum intersection angles, confirming that the actual flight path closely adhered to the planned trajectory, particularly with respect to pitch and roll angles. Instances where some points exceed the theoretical maximum intersection angle are likely due to variations in image orientation accuracy during the flight.In a few cases, tie points observed in only two images exhibited very high intersection angles; these were visually inspected and confirmed to be correct matches. However, significant gross errors - such as points reconstructed well above or below the ground surface - were also identified. These errors were consistently associated with tie points observed in only two images captured from the same viewing direction.The fact that the actual maximum intersection angles per tie point remain well below the theoretical maximum indicates a moderate utilization of the accuracy potential offered by oblique imagery, especially in terms of elevation accuracy.

3.3 Tie Point Multiplicity and Accuracy

Tie point multiplicity refers to the number of images contributing to the calculation of a 3D point, indicating how frequently a point is observed across different images. Fig. 5 illustrates tie point multiplicity, showing the distribution of tie points based on the number of contributing images.

Our previous study [6],along with many other studies, showed that tie points appearing in only two images contribute minimally to image orientation and camera calibration, as they provideno control along their epipolar lines and tend to be less reliable. Excluding such tie points from the bundle block adjustment can reduce the number of unknowns without compromising the overall quality, thereby improving accuracy and reducing processing time. In high-overlap UAV image blocks, where many tie points are captured from similar viewing directions, optimizing feature selection becomes particularly important.

The image residual statistics are presented in Fig. 5. The results were derived from the bundle block adjustment (BBA), in which affine and tangential distortion parameters were estimated in addition to radial distortion. This extended modelling reduced the random error component of the sigma naught from 1.383 pixels (with only radial distortion parameters estimated) to 1.296 pixels, while also helping to minimize systematic errors and reducing both image residuals and the object space error of ground control points (GCPs).To further evaluate spatial accuracy, GCPs were incorporated into the adjustment with a nominal precision of 5 cm in each coordinate, and the residuals were analyzed along the X, Y, and Z axes. The residual distributions exhibited mean values of −0.005 m, −0.008 m, and −0.041 m, with corresponding standard deviations of 0.053 m, 0.027 m, and 0.111 m, respectively. These results reflect high planimetric accuracy and acceptable vertical precision, confirming the reliability of the relative orientation and the overall adjustment quality.

The blue area between ±0.2 pixels in Fig. 5 highlight the trend of image residuals (and), indicating a reduction in systematic error. In contrast, when only radial distortion parameters were estimated, the residuals still exhibit noticeable variation(not shown in the graph). The purple lines in Fig. 5 represent the residual vector length ( ) per tie point, showing the group-wise average for tie points with the same multiplicity. As expected, the residual length increases sharply for 2-fold tie points and converges at higher multiplicities, except in cases with very few samples.The purple line with circles alongindicates the actual mean residual lengths obtained from the bundle block, while the purple line with triangles along represents the simulated results as described in Section 2.4.

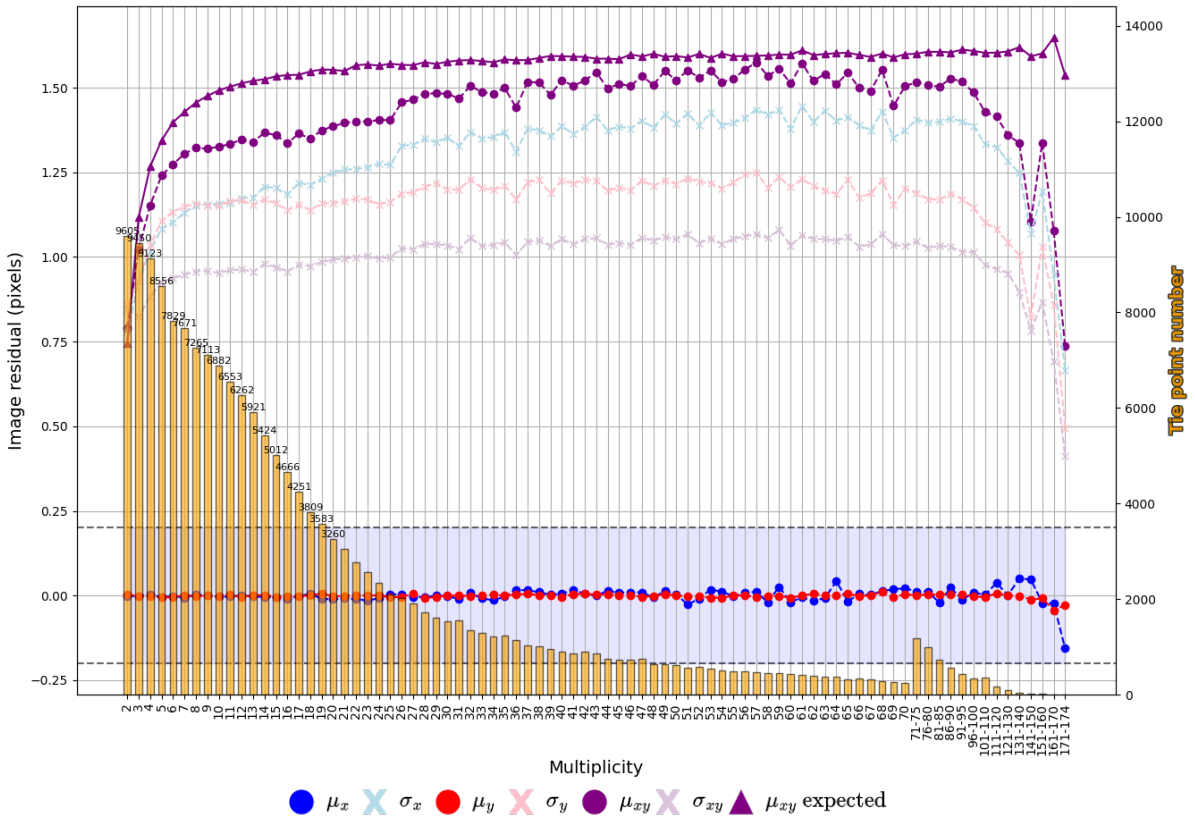

Fig. 5. Tie point multiplicity and image residual statistics in the penta-camera processing.

The simulated residuals, based on a normal distribution with zero mean and a standard deviation equal to the sigma naught of the original adjustment, closely follow the theoretical trend described in Section 2.4. This relationship is well illustrated by the purple line with triangles along, which aligns with the analytical expression for expected residual length as a function of tie point multiplicity. The model assumes ideal conditions, including random, independent errors and homogeneous measurement precision across all observations.

Notably, the comparison between simulated and actual results reveals that the real residuals are not normally distributed and exhibit clear deviations, suggesting that the underlying image observations are also not normally distributed. While the simulation follows a smooth, theoretical curve, the empirical data displaysclear deviations—indicating that key assumptions of the adjustment process (such as a correct functional and stochastic model, independence of observations, homogeneous measurement accuracy, and consistent interior orientation for each camera) are not fully satisfied. This highlights the need for improved stochastic models, which would lead to more accurate estimates of the unknown parameters.

4. Conclusions

In this paper, the computational factors influencing the performance of small-format multi-head camera systems were investigated, with particularemphasison image connectivity, image ray intersection angle, tie point multiplicity and accuracy. The findings reveal that image connectivity - both at the block level (super image connectivity) and within sub-areas (individual image connectivity) - is strongly influenced by image overlap.However, the relationship deviates significantly from direct proportionality due to viewing direction and

geometric configuration. Regarding the image ray intersection angle, the results show that the maximum values are generally consistent with theoretical expectations, confirming that the flight path closely adhered to planned parameters.Despite the use of algorithms designed to favor high-overlap regions, relatively few connections were observed between opposing oblique viewing directions. Nevertheless, the intersection angle analysis confirmed that tie point matches between different oblique views are indeed possible.In terms of tie point multiplicity and accuracy, results obtained from the bundle block adjustment (BBA), in which affine and tangential distortion parameters were estimated, demonstrated a reduction in sigma naught, a decrease in both systematic and random errors, and improved object space accuracy for ground control points. These results confirm the effectiveness and necessity of incorporating distortion modelling to enhance the reliability of relative orientation and the overall quality of photogrammetric adjustment. It is assumed that some of the remaining inconsistencies may be partially influenced by rolling shutter effects.

Overall, the results suggest several areas for improvement, indicating that the current camera configuration is not yet fully optimized. Future work will focus on evaluating the system's impact on computational aspects related to general-purpose mapping, while also exploring improvements in camera calibration procedures and the number and spatial distribution of ground control points (GCPs). Continued refinement in network design, matching strategy, and camera modelling is necessary to fully realize the potential of small-format multi-head camera systems for high-accuracy 3D mapping.

5. References

1. *Remondino, F., & Gerke, M. (2015, September). Oblique aerial imagery–a review. In Photogrammetric week (Vol. 15, No. 12, pp. 75-81). Wichmann/VDE Verlag.*
2. *Gerke, M., Nex, F., Remondino, F., Jacobsen, K., Kremer, J., Karel, W., ... & Ostrowski, W. (2016). Orientation of oblique airborne image sets-experiences from the ISPRS/EUROSDR benchmark on multi-platform photogrammetry. The International Archives of the Photogrammetry, Remote Sensing and Spatial Information Sciences 41-B1, 41, 185-191.*
3. *Toschi, I., Ramos, M. M., Nocerino, E., Menna, F., Remondino, F., Moe, K., ... & Fassi, F. (2017). Oblique photogrammetry supporting 3D urban reconstruction of complex scenarios. International Archives of the Photogrammetry, Remote Sensing and Spatial Information Sciences, 42, 519-526.*
4. Alsadik, B., Remondino, F., & Nex, F. (2022). Simulating a hybrid acquisition system for UAV platforms. *Drones*, *6*(11), 314.
5. *Bannakulpiphat, T., &Santitamnont, P. (2024). A Comparative Analysis of Camera Rig Parameters in Photogrammetric Software for Small-Format Oblique Camera System on Unmanned Aerial Vehicle. International Journal of Geoinformatics, 20(2), 1-10.*
6. *Bannakulpiphat, T., Karel, W., Ressl, C., & Pfeifer, N. (2024). Optimizing Bundle Block Adjustment for High-Overlap Small-Format Multi-Head Camera Systems. The International Archives of the Photogrammetry, Remote Sensing and Spatial Information Sciences, 48, 17-24.*
7. *Karel, W., Doneus, M., Verhoeve, G., Bries, C., Ressl, C., & Pfeifer, N. (2013). Oriental–Automatic Geo-referencing and Ortho-rectification of Archaeological Aerial Photographs. ISPRS Annals of the Photogrammetry, Remote Sensing and Spatial Information Sciences, 2, 175-180.*

8. *Fischler, M. A., & Bolles, R. C. (1981). Random sample consensus: a paradigm for model fitting with applications to image analysis and automated cartography. Communications of the ACM, 24(6), 381-395.*
9. *Karel, W., Ressl, C., & Pfeifer, N. (2016). Efficient orientation and calibration of large aerial blocks of multi-camera platforms. The International Archives of the Photogrammetry, Remote Sensing and Spatial Information Sciences, 41, 199-204.*